Crystallization of Polyethylene from Melt with Lowered Chain Entanglements

M. Psarski, E. Piorkowska, and A. Galeski*

Centre of Molecular and Macromolecular Studies, Polish Academy of Sciences, Sienkiewicza 112, 90 363 Lodz, Poland

Received March 1, 1999

ABSTRACT: A method of obtaining polymer with markedly decreased entanglements concentration in melt, via high-pressure crystallization of high-density polyethylene (HDPE), is elaborated. It is shown, by calculations and experiments, that melting of chain-extended crystals obtained in this process provides a chain-disentangled melt for a period of 20−30 min. The disentanglement is tested by means of spherulite growth rate measurements in a regime II melt crystallization. Spherulites grow faster from partially disentangled melt than from melt with normal concentration of entanglements: the growth rate is increased by 25−45%, and the conversion rate is also markedly higher. The difference is augmenting with decreasing undercooling—consistently with conclusions made from nucleation theory including reptation—and decaying with increasing time of melt annealing at 160 °C before crystallization, which is a result of entanglements reconstitution. The crystallization behavior in initially chain disentangled samples subjected to 25−30 min melt annealing is typical of entangled polyethylene, which indicates a complete entanglement restoration. The activation energy for reptation, determined from these data, is approximately 25 kJ/mol. Differences in overall isothermal crystallization kinetics of chain entangled and chain disentangled samples are considerable at moderate undercooling. The nucleation density during crystallization from disentangled melt is reduced in consequence of desorption of chains from heterogeneities surfaces during prior high-pressure crystallization of the samples. Melt annealing causes readsorption and restoration of normal nucleation density. The morphology of samples crystallized from a chain-disentangled melt is significantly different than those crystallized from a chain-entangled melt while the crystal thicknesses are similar.

Introduction

Entanglements between macromolecular chains, being one of the basic consequences of their considerable length, are very important and yet not fully understood from both fundamental knowledge and industrial applications perspectives. The mutual interpenetration of macromolecules determines the course of processes in which the substantial fragments of chains are involved. Some of the most significant examples of such processes are crystallization, flow of molten polymer, and mechanical deformation of solid polymers.

In this paper, a method is proposed and tested for obtaining linear polyethylene with markedly reduced entanglement concentration, in which disentanglement is still maintained for a period of time after melting. Such samples allow one for the first time to study the role of chain disentanglement in a molten polymer on the crystallization process and other properties.

The basic idea relies on melting differences of chain-folded and chain-extended crystals (CE). Melting of disentangled chain-folded polyethylene crystals leads to immediate reentangling. The effect is most probably due to chain folds present in polyethylene single crystals. The basal surface free energy of such crystals consists of the energy of folds, chain ends, and cilia. There are some arguments and also observations by Barham and Sadler[1] that chain-folded crystals "explode" upon melting and the fold energy is released in an explosive, springwise manner. Fragments and ends of chains incorporated in crystals are ejected with a high kinetic energy into the already molten polymer and interlace with other chains rapidly due to entropic force.

A quite different behavior may be expected if the chains in the CE crystals are not folded and the basal planes consist predominantly of chain ends. Such a crystal plane does not require relaxing of its energy on melting, and the chains are not supposed to be translocated to a large extent. The basic conformational change is then the entropy-driven coiling. Therefore, melting of such crystals does not increase significantly the number of entanglements over that resident in the amorphous phase of the polymer before melting. Furthermore, if the amorphous phase contains very few entanglements and/or the crystallinity level of the polymer is very high, melting should produce a melt with the average distance between entanglement knots, M_e, close to M. The disentanglements of the molten polymer should be maintained in the melt for a period of time related to the so-called Doi−Edwards disengagement time, i.e., the time needed for a macromolecule to reptate to entirely new position.

For a better understanding of the results, we present below briefly the main facts concerning entanglements and their role in crystallization of polymers.

Molecular Dynamics in Polymer Melts. The extent of chain entanglement is frequently described by the average molecular weight between entanglements, M_e, corresponding to the average chain fragment comprised between consecutive entanglement knots. The value of M_e, estimated on the basis of the network theory and compared with experiments (using the Ferry formula), is on the order of 10^3−10^4. For linear polyethylene $M_e = 1240$,[2,3] i.e., approximately 40 entanglement points for a PE chain of a molecular weight $M =$ 55 000.

The notion of entanglement describes the fact that the chains cannot cross each other in their transversal motion; therefore, neighboring macromolecules consti-

10.1021/ma990298h CCC: $19.00
Published on Web 01/11/2000

tute barriers for chain movement. Because of this confinement, represented as a reduction of number of available chain conformations, chain mobility in molten polymer is possible mainly via longitudinal movement. The environment constitutes an imaginary tube for a chain, in which the chain is trapped. Any large-distance movement of the chain, thermal movement or movement caused by an external stress, is allowed only along such a tube. The chain motion consists of three characteristic types: (A) The first is fast chain movements perpendicular to the tube axis, with short relaxation times, representing the dynamics of chain sequences shorter than the entanglement spacing along the chain—disentanglement from the neighbors is not required in this mode. The Rouse model describes this type of motion, with a characteristic relaxation time $\tau_e \propto \tau_s M^2$, where τ_s is the relaxation time defined in the monomeric scale, $\tau_s \sim 10^{-11}$ s (ref 4) and M is the molecular weight of the polymer. (B) The second is longitudinal fluctuation of the segment density, leading to tube length fluctuation, with a characteristic time $\tau_R \propto \tau_s M^2$, and (C) The last one is evolution of the axis of the tube, leading to disentanglement of the chain. Long relaxation times of this motion, $\tau_D \propto Z\tau_s M^2$, where $Z = M/M_e$, correspond to the influence of entanglements on chain mobility and are characteristic for curvilinear diffusion of a chain along a tube, called by de Gennes a "reptation". The concept of reptation is a basis for the theories of large-distance mobility of a chain trapped in entangled molten polymer, founded and developed mainly by de Gennes,[5] Edwards,[6] Doi and Edwards,[7] and Graessley.[8] According to this idea, only diffusing chain ends, which randomly choose the direction in space, can change the shape of the tube. This continuous process, called "tube renewal", leads to a complete disengagement of a chain from the tube and a new tube formation. The time for a complete renewal of the chain conformation, called reptation time, scales for long chains as τ_D. For chains of the average length, the number of entanglements along the chain, expressed as the ratio of the chain length to entanglement spacing, or M/M_e, has to be taken into account more deliberately. If this ratio is low, e.g., smaller than 100, the chain may form loops outside the tube, which leads to tube length fluctuation. As a result, the reptation time may be estimated as:[9,10]

$$\tau_{rep} \propto \tau_s M^3 \left[1 - \left(\frac{M_e}{M}\right)^{1/2}\right]^2 \qquad (1)$$

The expression (eq 1) is taken as an outset in this work. In a hypothetical polymer with no entanglements right after melting, the macromolecules are subject to thermal diffusion. As the chains diffuse between each other, the entanglements are gradually restored. The process of reentangling may be envisaged as a progressive formation of a tube for each chain. The time for a whole tube to be constructed may be roughly estimated by integration of eq 1 by M_e, decreasing with time from the initial value $M_e = M$ (no entanglements along a chain) to $M_e = 1240$ (PE melt with saturated level of entanglements).[11] In the case of a molecular weight on the order of 55 000 (the authors use such a commercial polymer in the studies), such a calculation gives the time for reentangling in the range 5−20 min. This result is in fair agreement with previous estimations: e.g., for UHMW−PE more than 10^4 s.[12,13] It is therefore conceivable that once we are able to obtain the initially disentangled polymer melt, the disentanglement should be maintained within a time scale that could have an important effect on the further behavior of the polymer and would allow for experimental evaluation of this effect.

Crystallization of Polymers. The crystallization of polymers starts at seeds. The nucleation model of the crystal growth, invented by Turnbull and Fisher for small molecules,[14] generally also applies to polymers. However, the whole process of crystallization is unique in macromolecular materials. Because of the low activity of the primary nuclei in polymers, a significant undercooling is required to start the crystallization, ranging from 10 to 100 °C with respect to the melting temperature. The growth of polymer crystals proceeds via the secondary nucleation mechanism and also requires a quite high undercooling. The hindrances to crystallization result from chain structure of macromolecules: their large length and mutual entanglement restrain their mobility to a great extent. Chain motion occurs mainly through reptation. Large-scale conformational chain rearrangements are required to shift small fragments of chains to suitable positions and incorporate them into growing crystal. Therefore, the mobility of a macromolecule with respect to its neighbors is crucial in polymer crystallization and requires a careful consideration in the description of nucleation and growth of polymer crystals.

Once nucleated, the polymer crystals grow. The growth results from a superposition of two competing processes: the secondary nucleation on the crystal face and the substrate completion. Their relative intensities vary with temperature, influencing the growth mechanism and, consequently, the structure and mechanical properties of the solid polymer. These essential differences give rise to a distinction of three regimes of crystallization.[15] At moderate undercoolings (in regime I and the upper region of regime II), the substrate completion rate is higher or comparable to that resulting from filling the layer with secondary nuclei. A macromolecule, once attached to a crystal face in a single nucleation event, is quite likely to be successively engaged in the layer formation, completing its substantial part. Crystal face layers are built up in a chain-folded manner, and—because large lengths of chains are involved—macromolecules are in great part reeled out of the melt by crystallization forces. In these circumstances, chain mobility is expected to influence markedly crystal growth. As the crystallization temperature is lowered (and regime III is approached), the crystal surface nucleation increasingly dominates the layer spreading process and the growth consists predominantly of profuse nucleation events. Macromolecules are embedded along their lengths in numerous crystal layers, frequently belonging to different crystals, and are subject only to small displacements in the course of crystallization. Thus, at large undercoolings the melt resistance to chain motions should not affect much the crystal formation.

The reptation model of polymer molecular dynamics[5] considers the fact that—due to the obstacles formed by the entanglements with other macromolecules—any motion transverse to the chain axis requires extensive cooperation from adjacent chains and is much more difficult than the longitudinal chain progression. The ease of reptational mobility, both thermal mobility and mobility under an applied force, is determined by the

resistance of the melt to chain motion, which—in turn—depends on the structure of the entanglement network: the entanglement topology and concentration. It is expected that the reduction of entanglement concentration, lowering the number of obstacles to chain motion, increases the rate at which the chain reptates. The effective reptational friction experienced by a chain, pulled by crystallization forces toward the growth front (in the reeling-in process), should therefore depend—apart from the pending chain length—on the concentration of entanglements and should decrease with the decrease of the later. As they arise from the reptation theory, the entanglement points act as obstacles, additional to friction, in the reptation of the chain. According to the kinetic theory of crystallization, the reptation rate has an effect on the crystal growth, particularly at low undercoolings. The effect of reeling-in rate on the crystal growth is expressed by the formula for the growth rate, G, given by Hoffman[16, 17] (for more detailed and precise discussion of polymer crystallization see recent review by Hoffman[18]):

$$G = G_0 \exp\left[-\frac{Q_D^*}{RT}\right] \exp\left[-\frac{K_g}{T\Delta T}\right] \qquad (2)$$

The $\exp[-K_g/T\Delta T]$ factor in this equation represents a stable secondary nucleus formation (T is the crystallization temperature, ΔT is the undercooling, and K_g is a constant depending on the crystallization regime). The $G_0 \exp[-Q_D^*/RT]$ factor characterizes the slowing down of the crystal growth caused by the resistance of the molten polymer to the pulling of the macromolecule by crystallization forces (Q_D^* is the activation energy for reptation; R is the universal gas constant). The preexponential factor G_0 is a function of $f/(\zeta_r n)$, where f is a crystallization force, n is the number of pendant chain units, proportional to M, and ζ_r is the reptational friction coefficient. The crystallization forces draw a macromolecule, or its part, adjoining the growing crystal, to the growth front. The resistance of the melt to this motion is greater the more entangled the chain with the surrounding macromolecules. At low undercoolings, as large fragments of chains are incorporated in crystals in a tight-folded manner, the resistance to chain transport controls the crystal growth, G. This reasoning implies that the lower the number of entanglements along the chains, the higher growth rate is possible at high crystallization temperatures.

The growth rate measured during isothermal melt crystallization at low undercooling can then help to detect changes in the level of entanglements in crystallizing molten polymer with respect to the saturated entanglement concentration. Spherulite growth rate, equivalent to that of lamellar crystals, can be measured by means of light microscopy, during isothermal crystallization. This procedure was first applied for testing the disentanglement in melts of chain-extended (CE) polyethylene obtained by high-pressure crystallization. The density of CE polyethylene materials can reach 0.994 g/cm^3, indicating almost no amorphous phase existence. Macromolecular chains in CE samples are then completely uncoiled and disentangled—internally and between other macromolecules. As the chains are straightened, the folding in CE crystals is scarce.

High-pressure crystallized chain-extended linear polyethylene was, therefore, chosen in this research as an initially disentangled material that should preserve chain disentanglement for a substantial time after melting. This hypothesis was verified by investigation of the kinetics of crystallization from such molten samples. Chain straightening in CE samples—occurring under high pressure and temperature, through chain slippage in the *condis* mesophase[19]—ensures a high level of disentanglement and a scarcity of chain folds in the solid state.

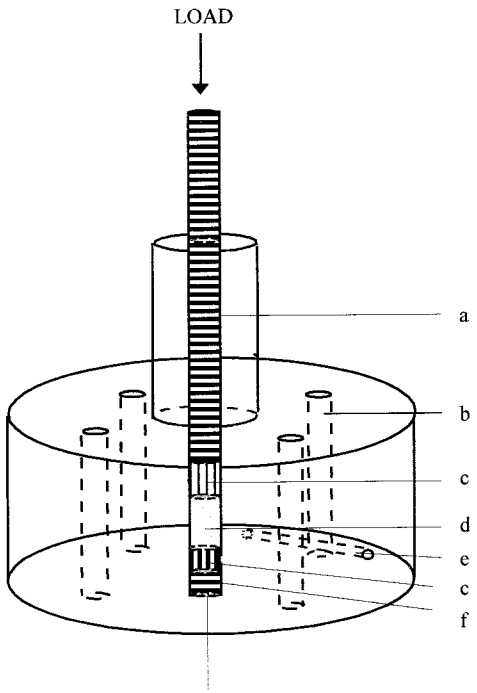

Figure 1. Pressure cell details: (a) pressing punch, (b) heater, (c) brass seals, (d) sample, (e) temperature sensor channel, and (f) closing punch.

Experimental Section

Linear polyethylene Petrothene LS 606−00, Millennium (former Quantum, VSI Division, Cincinnati, OH) was used in this study for preparing chain-extended as well as reference samples. Its weight-average molecular weight, $M_w = 55\,000$, polydispersity index, $M_n/M_w = 4.80$, melt flow index, MFI = 9−11 g/10 min (ASTM D-1238), and density is in the range 0.941−0.980 g/cm^3, depending on the crystallinity level. A narrow fraction of HDPE, $M_w = 88\,500$, $M_n/M_w = 1.11$, from S.N.P.A., was also used for a part of the research.

The samples in the form of 1 mm thick films were compression molded at a temperature of 160 °C under a pressure of 15MPa for 2 min and solidified at ambient temperature. Disks 9.5 mm in diameter were cut out from the films. About 20 such disks were loaded into a custom-made pressure-cell in which the high-pressure crystallization was conducted. The cell, shown in Figure 1, is made of ultrahigh-strength steel capable of applying pressure up to 1000 MPa, at a temperature of 300 °C. A channel is drilled along the axis of the cell, with very high surface smoothness (the channel surface roughness is 0.02−0.12 μm) and high diameter accuracy (the roundness of the hole deviation is 0.4−0.6 μm). Tungsten carbide punches, capable of pressure up to 1680 MPa, are used. The accuracy of fitting the punches to the channel and additional brass sealing prevents the highly compressed molten polymer from any leakage out of the cell. Four heaters, 600 W total power, are controlled by an Omega 9131A temperature controller, ensuring inside the cell a temperature accuracy of 1 °C. The temperature sensor is placed in a small channel drilled in the wall of the cell and located a distance of 10 mm from the sample. The polymer is compressed by use of an Instron tensile testing machine, via a fixture stabilizing the load exactly along

the die axis. The hydrostatic pressure inside the cell is controlled with an accuracy of about 0.5 MPa.

The high-pressure crystallization procedure, based on our earlier work,[20] was as follows: (1) melting the sample at atmospheric pressure at a temperature of 235 °C, (2) application of a pressure of 630 MPa, (3) crystallization for 1 h, (4) cooling the sample down to 60 °C still under pressure, and (5) release of the pressure.

The samples (marked as PECE) were obtained in the form of rods 9.5 mm in diameter, about 1 cm high. The process parameters were adjusted on the basis of a number of experiments, to minimize the extent of degradation of polyethylene.

To eliminate any effects other than chain extension and disentanglement on the properties investigated in further research, the reference samples were subject to the analogous thermal history as PECE samples: they were kept at a temperature of 235 °C for 1 h, but at a pressure of 250 MPa at which the pseudohexagonal phase and chain extension—according to the phase diagram of linear polyethylene—do not occur. The lower DSC melting points and, consequently, the thinner average lamellar thickness in these samples—labeled below as PEref—support this assumption. In Appendix I, other anticipated side effects in regarded experimental procedures are described in detail.

The habits of crystallization from melts of disentangled and reference samples were comprehensively studied. Spherulite growth rates during isothermal crystallization, preceded by melt annealing at 160 °C for different time intervals, were measured using light microscopy. The densities of primary nuclei active in such crystallizations were evaluated in bulk samples by means of light microscopy and compared to the results obtained from small-angle light-scattering experiments. The macroscopic isothermal crystallization kinetics and the influence of melt annealing on crystallization were studied by means of differential scanning calorimetry (DSC). The degrees of crystallinity of melt-crystallized samples were measured in the DSC and wide-angle X-ray scattering experiments. The morphological features of melt-crystallized samples—spherulitic structure and lamellar thickness—were investigated using light and atomic force microscopy and DSC.

Gel Permeation Chromatography. The GPC measurements were performed using a Waters 150-C apparatus equipped with a differential refractometric detector and Waters HMW-7 and HMW-6E columns at 142 °C. Samples were dissolved in 1,2,4-trichlorobenzene at 142 °C for 25 h.

Density Measurements. Densities of the samples were determined by means of a density gradient column, filled with a mixture of ethyl alcohol and water. Measurements were performed at 22 °C.

Light Microscopy. The crystallization from melts of the PECE and PEref samples was investigated by means of a polarizing light microscope equipped with a Linkam THMS 600 hot stage (controlled with a precision of 0.1 °C and overheating/overcooling during the change of the temperature profile of 0.1 °C) and connected to image acquisition and analysis system. The specimens, prepared by careful microtoming of PECE and PEref samples (sections 1μm thick), were placed between two small parts of the coverslips (ca 6 × 8 mm), which were then glued at the corners with epoxy resin. The thickness of the sections was adjusted to minimize the number of spherulite nuclei within the microscope field. Microtoming was preferred to pressing molten polymer between two coverslips, frequently employed in such measurements, due to undesirable orientation effects that may result from pressing the sample. Fixing the sections between glued glasses ensured the uniform thickness of molten specimens. The hot stage temperature profile employed consisted of (a) heating the specimen at a rate of 100 °C/min to 160 °C, (b) maintaining this temperature for a given melt annealing time (in the range 1−30 min), (c) cooling the specimen at −15 °C/min down to the chosen isothermal crystallization temperature (in the range 121−125 °C), and (d) maintaining the crystallization temperature until complete crystallization of the specimen is reached. The course of crystallization was recorded, and the spherulite dimensions were measured, using an image analysis system. The growth rates were calculated as the slopes of the spherulite radius vs crystallization time plots, constructed on the basis of sequences of micrographs.

Nucleation density was estimated on the basis of observations in polarizing microscope of 7−10 μm thick sections, cut from bulk PECE and PEref samples, melt annealed at 160 °C for 2−30 min and crystallized isothermally at 123 °C in the DSC apparatus. The microtoming introduced some compression of the specimens, which was reduced by heating the specimens at 50−55 °C for a short time (in order to straighten their folded surface) and by means of silicone oil immersion. The average nucleation density, D, was estimated as a proportion of the total number of spherulites, N_s, that could be resolved in PECE or PEref specimens to their relevant total area.

The calculations were performed on the basis of a large number of measurements (∼50). The values of the area were corrected for that specimen compression during microtoming that could not be eliminated. The dimensions of the ready to microscope observation sections were compared with those of the trimmed specimen block surface being cut, measured during microtoming, and the correction was made on this basis. Average spherulite radii, $\langle R \rangle$, were also calculated from the above data.

Differential Thermal Analysis. The thermal analysis of the samples was conducted using a TA 2010 DSC apparatus (TA Instruments, Inc., New Castle, DE), indium calibrated. Small pieces, of a total mass of 7 mg, were cut from the compressed rods, placed and pressed slightly into aluminum pans, to ensure good thermal contact with the DSC cell surface. The samples of virgin polymer were cut into the shape of a disk from films prepared by compression molding as described above. The melting thermograms were recorded at a heating rate of 10 °C/min, under nitrogen flow. The crystallinity levels and lamellar thickness, l^*, were estimated on the basis of heat of fusion of the sample ΔH_m recorded during heating the samples from a temperature of 60 to 170 °C and from the recorded melting temperature, T_m. For l^* the following equation was used:[21,22]

$$l^* = \frac{2\sigma_e T_m^0}{\Delta h_f (T_m^0 - T_m)} \tag{3}$$

where σ_e is a lamellar basal surface free energy (for PE $\sigma_e = 9 \times 10^{-6}$ J/cm^3), Δh_f is the heat of fusion per unit volume (for PE $\Delta h_f = 280$ J/cm^3 (ref 23), T_m^0 is the extrapolated equilibrium melting temperature, determined for the polyethylene used in this study, employing the Hoffman−Weeks method, as $T_m^0 = 145.1$ °C.

The isothermal crystallization runs, performed in the DSC apparatus, consisted of (a) heating the samples at 80 °C/min up to 160 °C, (b) maintaining the temperature for 2 min, (c) cooling the samples at −80 °C/min down to the crystallization temperature T_c, and (d) keeping the samples at T_c until no trace of crystallization thermal effect could be resolved. For the Hoffman−Weeks plot construction, the samples were then immediately heated at 10 °C/min to 160 °C and the melting endotherms were recorded.

X-ray Scattering. A MBraun (Austria) SWAX camera, utilizing conventional Kratky collimation system, was employed in this research. The front of the camera was directly mounted on the top of the tube shield of a stabilized Philips PW 1830 X-ray generator. The X-ray tube was operated at a power of 1.5 kW. Cu Kα radiation was used; monochromatization was performed by a Ni β filter and pulse-height discrimination. The entrance slit was adjusted to 50 μm. The radiation scattered at small (SAXS) and wide (WAXS) angles was recorded in acquisition time of 900s by means of a MBraun linear position-sensitive detector, model PSD 50. The detector had 1024 channels with a channel-to-channel distance of 52 μm. The experimental curves were corrected for sample absorption and desmeared from collimation distortions by means of the computer program 3DVIEW supplied by MBraun.

A part of the WAXS measurements was performed using a computerized diffractometer constructed in our laboratory on the basis of a DRON - 2.0 apparatus (USSR), (the Cu Kα line, generated at 30 kV and 10mA, filtering by a Ni β filter, and a pulse-height discrimination.).

The values of the long period, L, were evaluated on the basis of the scattered intensity patterns using the formula:

$$L = \frac{\lambda}{2 \sin \theta_{max}} \quad (4)$$

where λ is the X-ray wavelength ($\lambda_{Cu\ K\alpha} = 0.154$ nm) and θ_{max} is the scattering angle corresponding to the first-order maximum in the SAXS pattern.

The degrees of crystallinity were assessed on the basis of the WAXS profiles using a procedure of separation of the amorphous halo and reflections originating from main crystallographic planes of the lattice, described in detail in ref 24.

Atomic Force Microscopy. The morphological features of PECE and PEref samples were investigated by means of atomic force microscopes: Nanoscope III (Digital Instruments, Santa Barbara, CA) and the other constructed in the Physics Department of the University of Lodz, Poland, both using Si_3N_4 tips. The samples were cut from the central parts of compressed rods and extracted from the pressure cell, and their surfaces were microtomed and etched at room temperature with potassium permanganate dissolved in a mixture of sulfuric acid and orthophosphoric acid, following the method developed by Sheiko et al.[25] The scans were performed in air. The height and deflection mode images were recorded simultaneously.

Molten and then isothermally crystallized PECE and PEref samples for the AFM investigations were prepared in the hot stage in the form of films crystallized isothermally without the top coverslip. Small chunks of the material were heated to 160 °C at 80 °C/min, kept at this temperature for 2 min (30−60 μm thick films were obtained as a result of pressing of molten specimens at this step), cooled at −65 °C/min to 123 °C, kept at this temperature for 10 min (a time sufficient for a complete crystallization of the sample), and cooled at −65 °C/min down to the room temperature.

Results and Discussion

Spherulite Growth Rate. As it arises from the characterization of the high-pressure crystallized samples used in this research (see Appendix II), the chains constituting their crystalline phase are straightened to a large extent. As the chains within the CE crystals are disentangled and the share of the amorphous phase in PECE samples is very small, a conclusion is drawn that the entanglements in these samples are nearly eliminated and the first step of this research—a bulk solid largely disentangled polyethylene sample containing a very small amount of chain folds—is achieved. The crystal growth rate, reflected by the growth rate of the spherulites, can be measured directly by means of light microscopy. The measurements of spherulite dimensions vs time were conducted for the isothermal crystallization from melts of PECE and PEref samples. The crystallization temperature range applied, 121−125 °C, covering almost the entire regime II of crystallization of polyethylene, was imposed by the nature of the crystallization of polyethylene and experimental limitations. At lower T_c, a fine-grained spherulitic structure is formed due to high nucleation density, and the exact measurements are not possible. At 125 °C a crossover from spherulitic to axialitic morphology was observed, characteristic at temperatures in the region of the regime II−regime I transition.[26] At even higher temperatures, only randomly oriented lamellar crystals grew, eventually forming a dendritic structure or in some cases axialites.

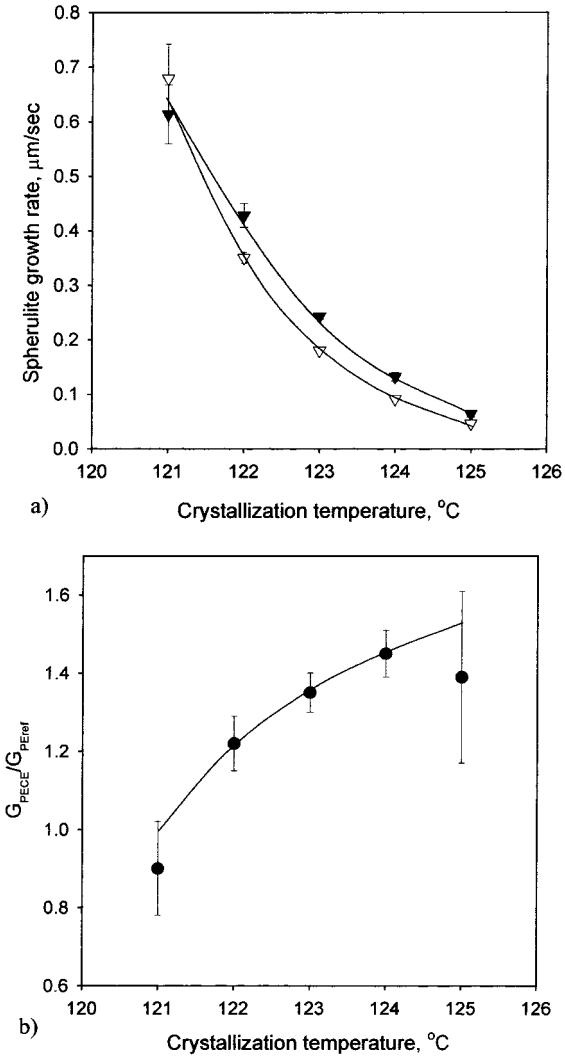

Figure 2. Spherulite growth rate in isothermal crystallization from melts of chain-extended (G_{PECE}) and reference (G_{PEref}) HDPE Petrothene samples vs crystallization temperature, T_c, shown as (a) the average values of G_{PECE} and G_{PEref} vs T_c and (b) the proportion of G_{PECE} to G_{PEref} vs T_c.

The average growth rates, calculated as the slopes of the spherulite radius vs crystallization time plots, are shown in Figure 2. The increase in the growth rate from the PECE melt, G_{PECE}, over that measured in reference samples, G_{PEref}, is observed. The increase is particularly significant at higher T_c, reaching 45% at 124 °C. As the crystallization temperature is lowered, the difference decreases down to 22% at 122 °C.

The reasoning presented in the Introduction to this paper implies that the lower the number of entanglements along the chains, the higher growth rate is possible at high crystallization temperatures. In accordance with the above rationale, a faster growth rate is a consequence of chain disentanglement, which apparently is preserved in the melt after melting CE PE crystals. This conclusion is also supported by the fact that the effect is smaller at lower T_c: during fast crystallization, caused primarily by more numerous secondary nucleation, shorter fragments of chains are incorporated in particular lamellar layers and the chain extraction from the melt is slight (the number of tight

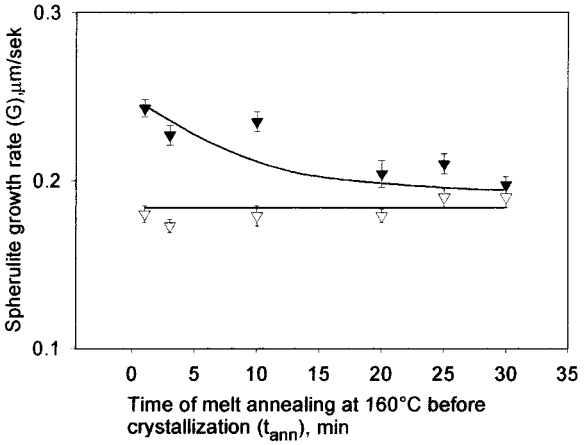

Figure 3. The average growth rates in crystallization at T_c = 123 °C vs melt-annealing time, t_{ann}.

folds in crystals is small). The influence of disentanglement on the growth rate then decreases.

As the spherulite growth is sensitive to the entanglement concentration in the melt, the growth rate measurements may also be applied for tracing the reconstitution of the entanglements in molten polymer. The procedure of such experiments requires an additional stage to the reported above isothermal crystallization experiments: keeping the sample in the molten state for a given time, before crystallization. The average growth rates measured for crystallization at the T_c = 123 °C, after annealing the melts of PECE and PEref samples at 160 °C, are shown in Figure 3 vs melt annealing time, t_{ann}. A decrease in G_{PECE} with t_{ann} is apparent from this plot. After 20 min of melt annealing, the growth rate in the PECE samples decreases significantly, keeping the PECE samples at 160 °C for 30 min causes a drop in the G_{PECE} values down to these measured for PEref. Longer annealing of the melt resulted in partial thermal degradation of the polymer. The drop in G_{PECE} values with melt annealing time represents the dynamics of renewed interlacing and entangling of initially disentangled chains, resulting from thermal diffusion of macromolecules. The time for a recovery of a saturated entanglements concentration in molten polyethylene at 160 °C, deduced from the above measurements, is in agreement with the estimate made in this work on the basis of the reptation time. The spherulite growth rate was measured during isothermal crystallization after fast melting of PECE and PEref specimens and maintaining the specimens at 160 °C for the desired melt annealing time.

In all cases of both types of samples examined, the spherulite growth was found to be linear with crystallization time, which was usually below 1 min. However, in a couple of specimens, where longer crystallization could be recorded at 126 °C, the growth is no more linear (see parts a and b of Figure 4) A decrease of the growth rate can be detected as early as 20 min after the start of crystallization. The growth slows down from that moment and finally, approximately after 45 min, assumes a rate comparable to that in PEref samples. The growth does not slow below G_{PEref} for longer crystallization time, up to 70 min. In contrast to PECE samples, the growth rate measured from the longest crystallization runs that could be recorded in PEref specimens (only up to 33 min, due to higher nucleation density) proved to be constant within the whole crystallization time (see Figure 4c). It should be noted that the constant value of G_{PEref}, as well as no traces of change in color of any specimen after crystallization at 126 °C, testifies that no thermal degradation or oxidation affected the samples during quite a long exposure to the crystallization temperature (a nitrogen flow over the specimens was always applied in these runs).

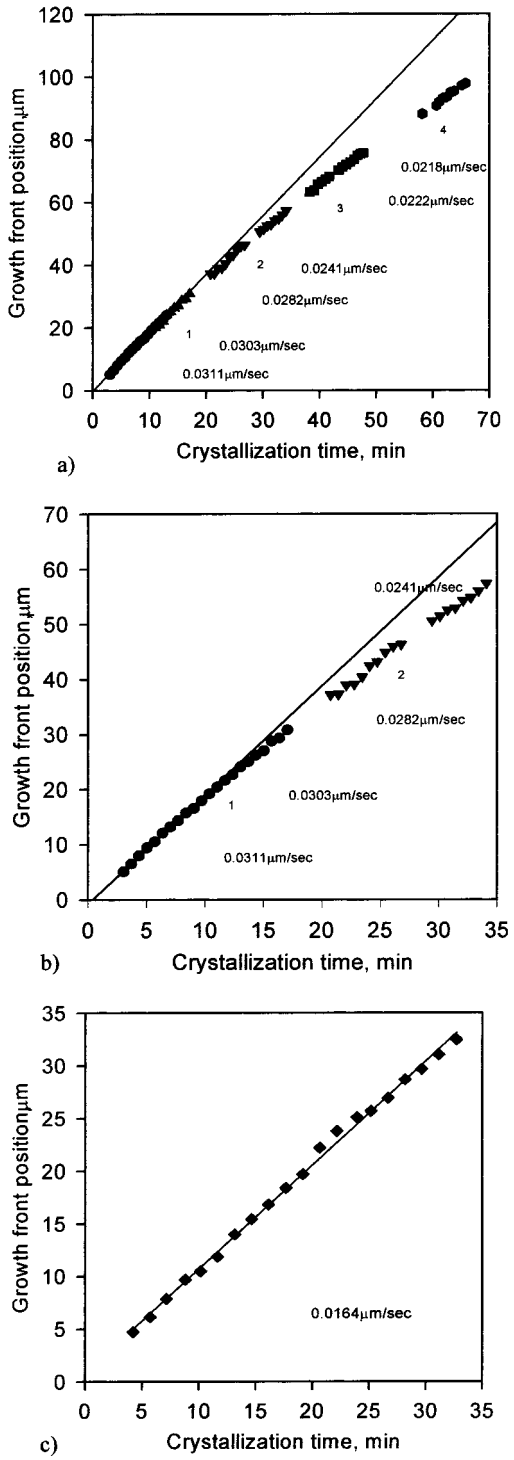

Figure 4. Spherulite growth rate in isothermal crystallization from melts of chain-extended (a and b) and reference (c) HDPE Petrothene samples vs crystallization time, t_{cryst}. The crystallization time is measured from the start of isothermal crystallization, the measurements in plots a and b are performed in consecutive time intervals on four spherulites growing near each other. The plot in part b shows data from part a, rescaled to compare with the plot in part c.

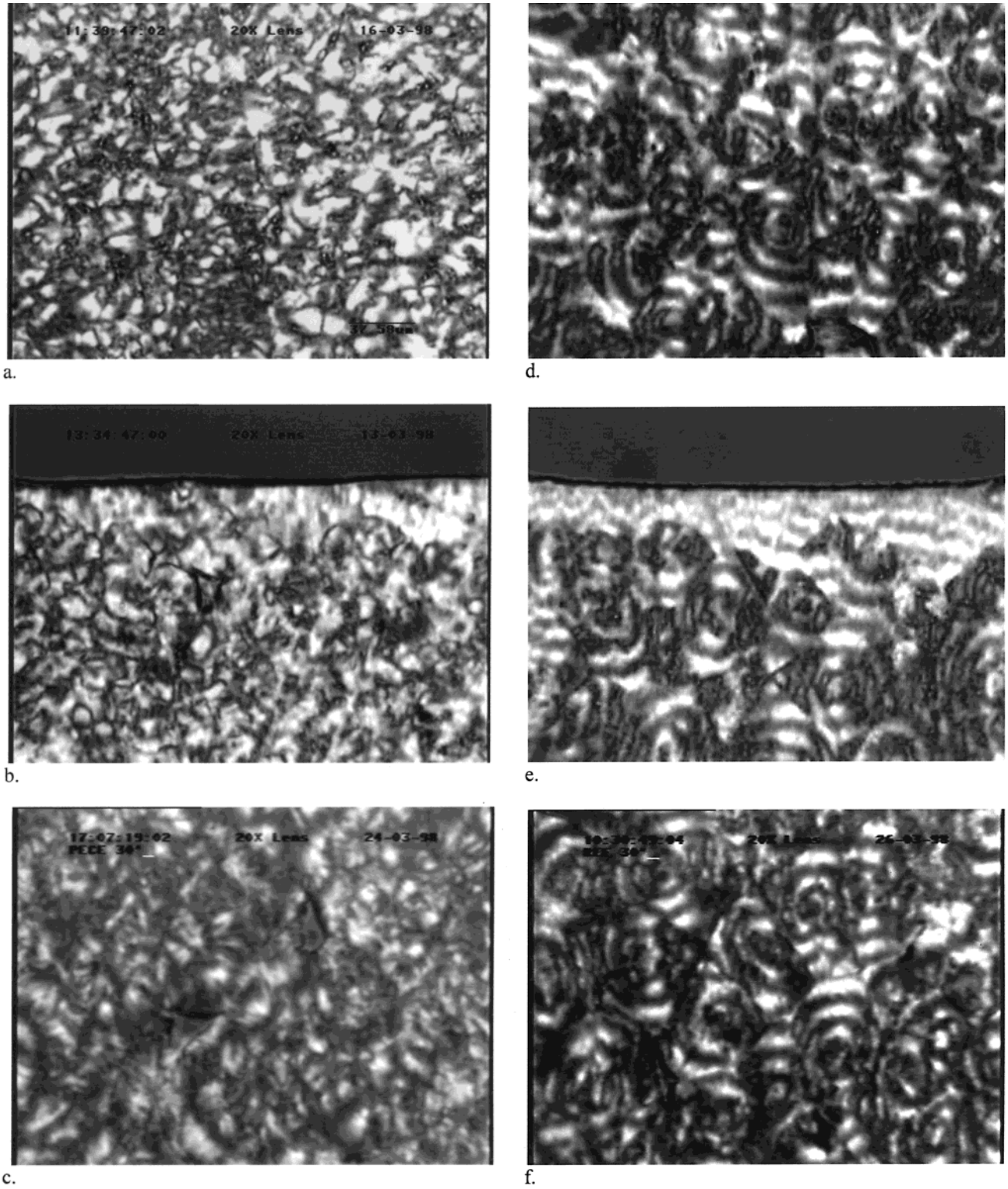

Figure 5. Polarized LM micrographs recorded for sections cut from PECE (a−c) and PEref (d−f) samples crystallized at 123 °C. The samples were melt annealed prior to crystallization at 160 °C for 2 min (a and b) and for 30 min (c). The sample border and thin transcrystalline layers resulting from surface nucleation of aluminum DSC pan are visible in parts b and d.

It is known from early works of Bassett,[27] Wunderlich, and others[28] that chain-extended crystallization is accompanied by molecular fractionation, i.e., chain-extended crystals, if crystallized for long time, are built from molecules of similar length. However, the crystals in PECE samples used in this study are not of uniform thickness, as it is seen in their AFM images (see Figure 17a in Appendix II). The crystal thickness varies within the same crystal, which means that each crystal is built from molecules of various lengths and the chain ends are not forming completely flat crystal surfaces. For comparison in Figure 17b the AFM images of chain-extended 88 500 fraction are presented. It is seen that here the surfaces of lamellae are flat and crystals are built of chains of equal molecular weight. It follows then that the localized fractionation in samples crystallized

Table 1. Average Nucleation Densities, *D*, and Average Spherulite Radii ⟨*R*⟩ of PECE and PEref Polyethylene Samples As Determined from Light Microscopy Examination

	PECE		PEref		
t_{ann}, min	D_{PECE}, 10^{-4} μm^{-2}	$\langle R_{PECE}\rangle$, μm	D_{PEref}, 10^{-4} μm^{-2}	$\langle R_{PEref}\rangle$, μm	D_{PEref}/D_{PECE}
2	2.39	36	4.43	27	1.85
20	3.26	31	4.11	28	1.26
30	3.18	32	2.99	33	0.94

under pressure for only 1 h is rather limited. The effect of localized fractionation on melt crystallization of PECE samples should not then be very significant. It could result in accelerating of the spherulite growth rate only if PE fractions from 8000 to 17000 are forming a continuous phase while the rest of the molten material is dispersed in the 8K−17K melt. The last suggestion follows from the fact that only 8K−17K PE fractions crystallize faster than the other fractions within the range of 120−128 °C (see ref 29 for extensive data on crystallization of PE narrow fractions). However, in such a case the difference in growth rates between hypothetical fractionated melt will be even enlarged at the lower limit of the temperature range (120−121 °C). This effect is just opposite to that observed for melt-crystallized PECE samples. Therefore, the faster crystal growth rate in melt-crystallized PECE samples over PEref samples is not caused by localized fractionation and should be attributed to disentanglement.

The decrease in G_{PECE} with time is then the result of thermal reptative chain entangling in melt. Since the self-diffusion coefficient decreases with decreasing melt temperature—thermal diffusion is slower in melt at crystallization temperatures of 126 °C than in the melt at 160 °C. The estimations of times required for a complete entanglement reconstruction—25 min at 160 °C and 45 min at 126 °C—are the basis for evaluation of the activation energy for reptation. It yields a value of 25 kJ/mol. This value, although quite rough, is in a fair agreement with the literature data, obtained from the long-chain molecule diffusion through bulk polyethylene experiments, at a level of 29.3 kJ/mol.[30]

Spherulite Nucleation Density. Observations of molten PECE and PEref specimens during melt annealing did not reveal any traces of birefringence, which indicates that no remnants of crystal aggregates remain after melting. Growing spherulites appeared almost simultaneously within the microscope field, both in PECE and PEref samples; however, a significantly smaller number of them were usually observed in PECE samples. The primary nucleation in polyethylene is very intense, and a large number of small spherulites are a common morphological feature for this polymer (the average spherulite radius in a bulk Petrothene polyethylene sample crystallized at 124 °C is on the order of 10 μm[31]). The geometry of crystallization in 1 μm thick film is essentially two-dimensional and the number of spherulites seen in microscope field should be small. However, a slight increase in specimen thickness and—consequently—in the observed polymer local volume, results in a significant increase in the number of spherulites seen, overlapping each other.

The concentration of nuclei observed in most specimens was increased even more by the surfaces of glass slips' nucleation activity, which is remarkable in the case of polyethylene.[32] The growth centers location was usually reproducible in repeated melting−crystallization runs performed on the same specimen. The brand of glass slips used for the research was chosen so as to minimize the surface nucleation effect.

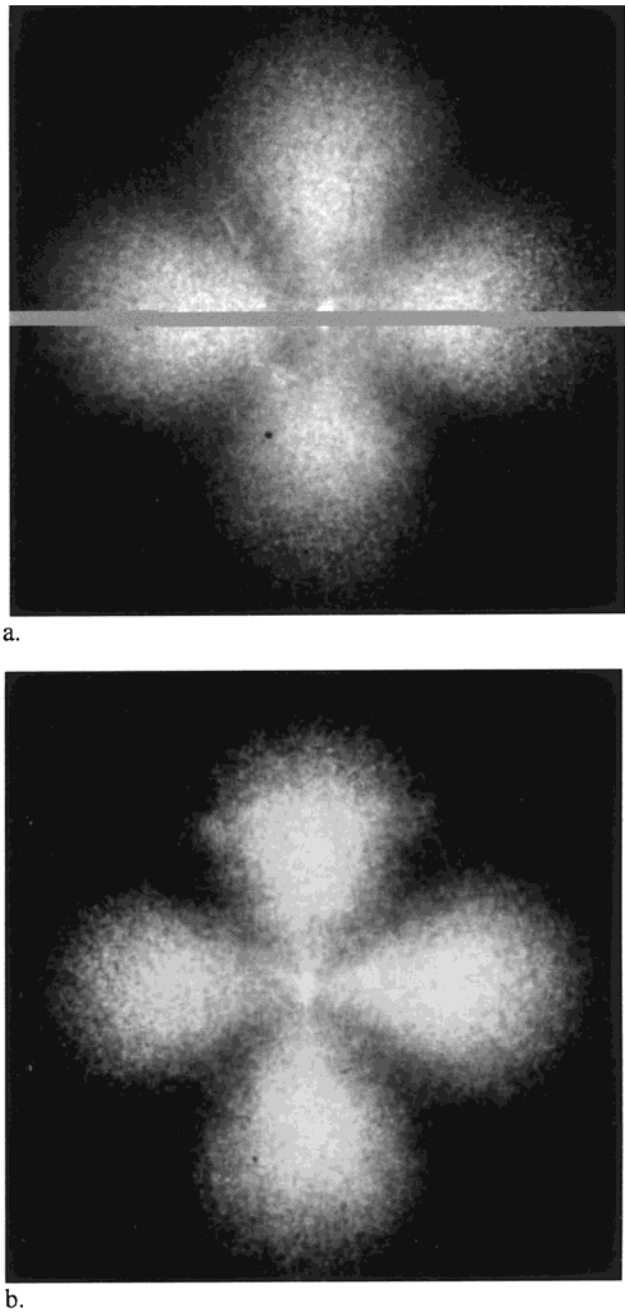

Figure 6. SALS patterns recorded for (a) PECE and (b) PEref samples.

The average spherulite dimensions and nucleation density in samples crystallized isothermally from entangled and disentangled melts were analyzed by means of light microscopy.

Exemplary micrographs of 7−10 μm thick sections of melt crystallized at 123 °C PECE and PEref samples, taken on a polarizing microscope, are shown in Figure 5. The spherulitic structure in these samples is discernible, although a remarkable difference between the PECE and PEref samples is apparent (see Morphology of Melt-Crystallized Samples section). Spherulite borders in PECE samples could often be distinguished only by means of rotating the polarizer and observing the changes in morphological features appearance.

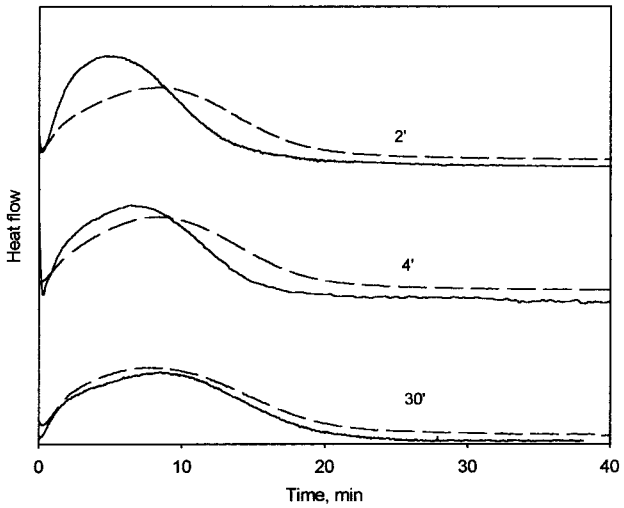

Figure 7. DSC thermograms of PECE and PEref polyethylenes recorded during isothermal crystallization at 123 °C after different melt annealing times: 2, 4, and 30 min at 160 °C. Solid lines are for PECE samples; dashed lines are for PEref samples.

The values of average nucleation densities, D, and average spherulite radii $\langle R \rangle$, calculated for samples crystallized from PECE and PEref melts, as well as proportions between primary nucleation density in both kinds of samples, are shown in Table 1. The specimen compression was considered in the calculations as described in the Experimental Section.

The nucleation densities in films obtained by fast crystallization from PECE and PEref material were also determined. The films were prepared by compression molding between chromium-plated brass 0.5 mm thick plates after a short exposition to 160 °C (0.5 min) in the press and then cooled in iced water. On the basis of the SALS experiments (see Figure 6), a proportion between primary nucleation densities in PECE and PEref films was calculated: $(D_{\mathrm{PEref}}/D_{\mathrm{PECE}})_{\mathrm{SALS}} \approx 1.76$. This value corresponds approximately to $(D_{\mathrm{PEref}}/D_{\mathrm{PECE}})_{\mathrm{LM}} \approx 1.85$ obtained from light microscopy measurements (see Table 1). Primary nucleation in the crystallization of polyethylene from chain-disentangled melt is therefore much less intense than in the case of a normally entangled melt. A similar finding has been previously reported for a different grade of HD-PE (Lupolen 6011L, BASF).[33] Light microscope measurements also show that melt annealing of PECE samples before crystallization leads to a gradual increase in D_{PECE}, and eventually, after $t_{\mathrm{ann}} \approx 30$ min, D_{PECE} becomes comparable to D_{PEref}.

A smaller number of nuclei in PECE with respect to PEref samples can be interpreted in terms of the heterogeneous character of the nucleation process. Nuclei are formed by proper alignment and orientation of large fragments of macromolecules adsorbed on the heterogeneities' surfaces. During high-pressure crystallization of polyethylene, chain desorption from some heterogeneities may occur − due to increased chain mobility in the *condis* phase—inactivating a part of heterogeneous nuclei. As a result, primary nucleation density during crystallization from melt of such a material is reduced. A prolonged maintaining of PECE sample in the molten state leads to renewed adsorption of polyethylene macromolecules on inactivated in the *condis* phase heterogeneities and the nucleation density during subsequent crystallization increases.

Macroscopic Crystallization Kinetics. Isothermal crystallization from melts of PECE and PEref samples at $T_c = 123$ °C was investigated by means of differential scanning calorimetry. Similar to the case of growth rate measurements, the melt was kept at 160 °C for various time intervals before crystallization in order to study the influence of melt annealing on crystallization kinetics. The exotherms recorded during crystallization runs after different melt annealing times, t_{ann}, are shown in Figure 7.

As can be seen from this figure, crystallization in bulk samples is much longer than in thin films used for the LM observations—the overall crystallization time in DSC runs is up to 30 min, while it is on the order of several minutes in hot stage crystallization. The difference is due to the strong nucleation activity of glass slips, which increases drastically the number of spherulites growing in thin films and thus shortens the overall crystallization time.

The surface nucleation, however, does also affect crystallization in bulk samples. The apparent change in the slope of the left wing of the thermograms, particularly significant in the case of PEref samples, can be attributed to nucleation caused by the surfaces of the aluminum DSC pans (see the Experimental Section)—in addition to nucleation in the bulk polymer. As it arises from the experimental observations and theoretical analysis,[34,35] the shape of the initial part of the conversion rate curve is influenced by the relation between the intensities of the surface and bulk nucleations.

The differences between crystallization of PECE and PEref samples are considerable. For t_{ann} up to 20 min, the heat flow recorded during crystallization of PECE samples—corresponding to the conversion rate—is always higher than in PEref samples. The total crystallization time, on the other hand, is shorter in PECE samples—crystallization from disentangled melts is apparently faster. However, as t_{ann} is increased, a change in the shape of PECE thermograms occurs and crystallization of PECE samples is progressively retarded. After melt annealing has taken place for $t_{\mathrm{ann}} =$ 30 min, a unification of the crystallization kinetics of both kinds of samples is apparent. Thus, analogous to growth rate measurements, the macroscopic crystallization kinetics investigation also reveals a distinct difference between crystallization from entangled and disentangled melt, diminishing with the time of disentangled melt annealing—the disentangled chains reentangle.

Also the bulk nucleation density characteristic for the brand of PE used is restored in PECE samples after 30 min of melt annealing at 160 °C.

It is concluded that these results agree well with the data obtained from independent measurement of the growth rate vs time of melt annealing, for which the time of re-entangling was determined at a level of 25 min. Also the time for restoring the nucleation density in PECE samples to the level exhibited by PEref samples, determined as 25 min, fits the melt-annealing time required for the unification of the crystallization of PECE and PEref samples.

Morphology of Melt-Crystallized Samples. To investigate the influence of entanglements of PE chains on the ability to form the crystalline phase, the weight degrees of crystallinity of samples crystallized isothermally at 123 °C from PECE and PEref melts were

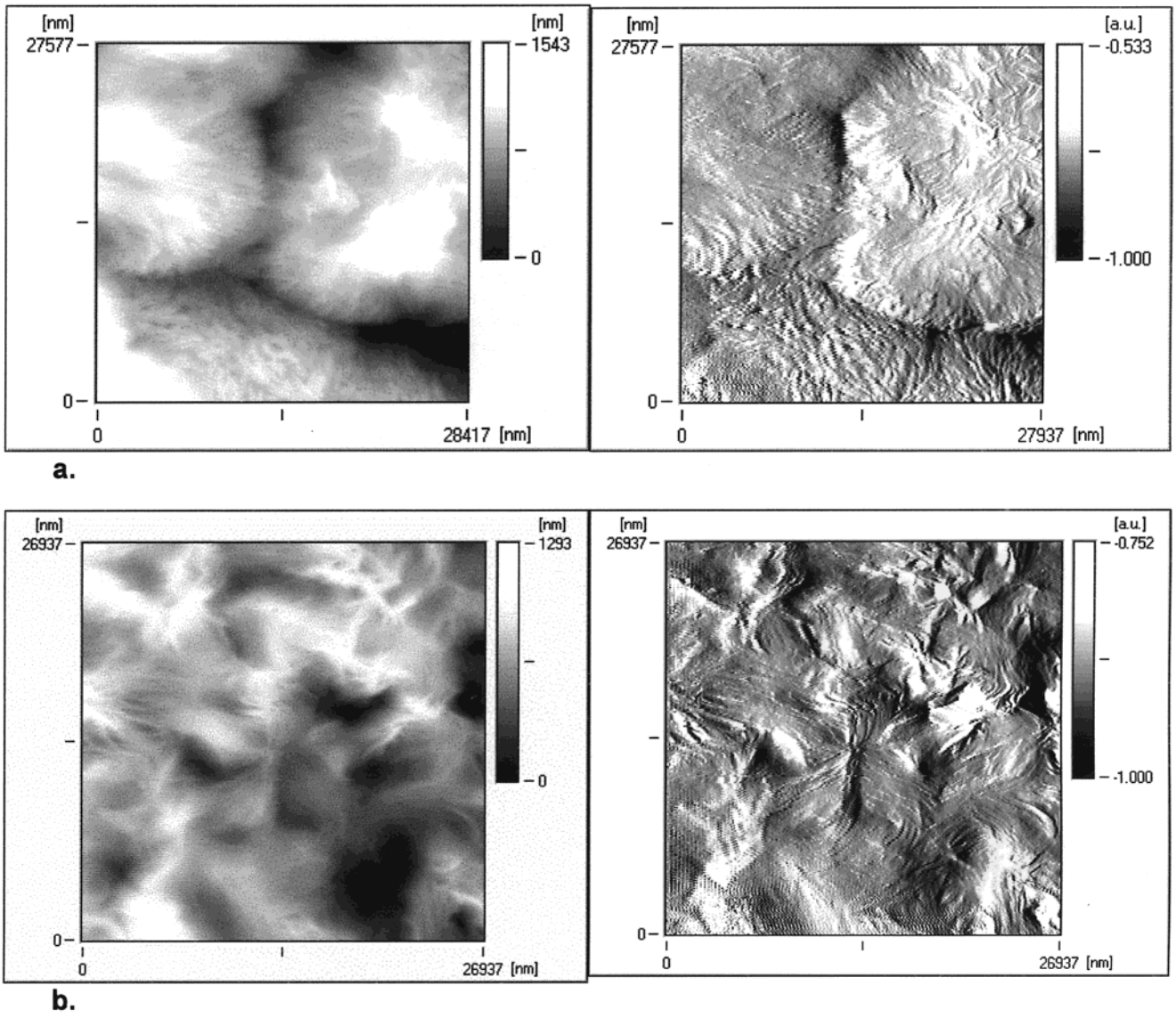

Figure 8. Spherulitic structure in PEref (a) and PECE (b) samples crystallized isothermally at 123 °C as revealed by the AFM observation. Left-hand side pictures are height images; right-hand side pictures are lateral force images.

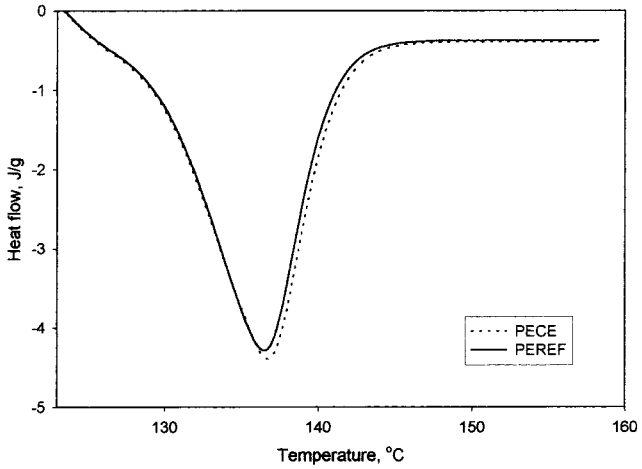

Figure 9. DSC melting endotherms of PECE and PEref samples crystallized isothermally at 123 °C.

calculated on the basis of the DSC isothermal crystallization and melting thermograms. The crystallinities achieved after short (1.5 min) melt annealing are slightly greater in PECE samples: X_c^{PECE} = 68.7 wt %/69.4 wt % and X_c^{PEref} = 66.4 wt %/66.4 wt %, as determined from the thermograms of crystallization/melting directly from crystallization temperature, respectively. Melt annealing of PECE samples before crystallization results in a gradual decrease of this difference and for the annealing time of 30 min X_c^{PECE} = 65.3 wt % and X_c^{PEref} = 66.0 wt %.

The supermolecular structure of melt-crystallized PECE and PEref samples was investigated by means of light microscopy and atomic force microscopy. The LM observations of sections taken from bulk samples, (see the Spherulite Nucleation Density section) reveal significant morphological difference between both kinds of samples (see Figure 5). The spherulitic-banded structure is readily discernible in PEref samples. The band period is about 14 μm and is independent of the time of melt annealing at 160 °C prior to crystallization. In PECE samples, spherulites are less evident, and their borders are not well visible. Spherulite banding cannot be detected. With increasing melt-annealing time, the spherulitic structure becomes better resolved and traces of banding of long spacing can be distinguished.

The AFM images of the surfaces of melt-crystallized PECE and PEref samples also exhibit a well-developed

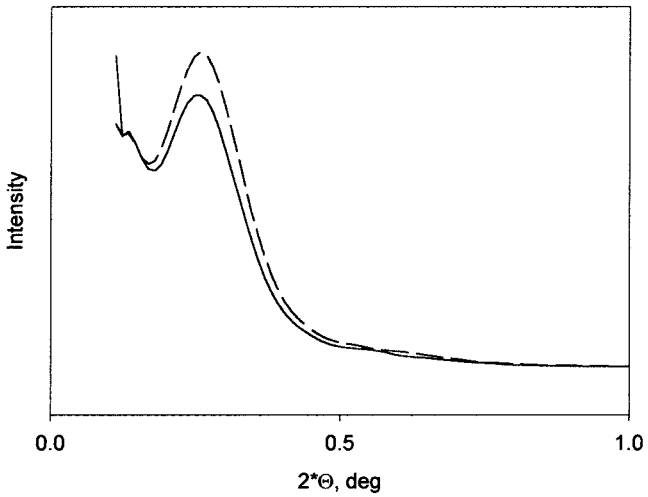

Figure 10. SAXS patterns recorded for PE samples isothermally crystallized at 123 °C from PECE (—) and PEref (- - -) melts, after 1.5 min of melt annealing at 160 °C.

spherulitic structure in PEref samples (Figure 8). However, due to intense surface nucleation of glass slips on which the specimens were prepared, the spherulites are much smaller than these in bulk samples crystallized at the same temperature—the radii are on the order of 5 μm. Similar to the LM observations, spherulites in PECE samples appear much less perfect. The spherulite centers are visible, but the radial arrangement and the borders are not well discernible in all directions with respect to the centers.

The average thicknesses of the lamellae in isothermally melt crystallized at 123 °C PECE and PEref samples, after 1.5−2 min of melt annealing at 160 °C, were compared on the basis of the DSC, SAXS, and AFM measurements.

The DSC heating at 10 °C/min runs were performed on isothermally crystallized samples (see the Macroscopic Crystallization Kinetics section), directly from the crystallization temperature. The endotherms recorded do not exhibit any significant differences in the shape and positions of the melting peaks of both kinds of samples (Figure 9). This indicates that the distribution of the lamellae thicknesses and their average values are similar in PECE and PEref melt-crystallized samples. The average lamellar thickness, estimated on the basis of the melting peak position, using expression 3, is 31.5 nm for PECE samples and 34.8 nm for PEref samples.

The SAXS patterns recorded for the PECE and PEref melt-crystallized samples are shown in Figure 10. The positions of the first-order maxima are similar, and the values of the long period, obtained from the analysis of the profiles, are 34.3 nm for both PECE and PEref samples. This result also shows that lamellae of similar thicknesses form in crystallization from melts of PECE and PEref samples.

The crystal sizes in melt-crystallized PECE and PEref samples were investigated directly by means of atomic force microscopy. Typical features of the lamellar morphology were revealed, and contrary to the spherulitic structure observations described above, no remarkable differences at this level showed up (see Figure 8). The methods of measurement were chosen so as to eliminate the tip shape convolution with the surface features on the nanometer length scale. Regions of specimens where flat-on lamellae formed terrace structures were picked (see Figure 11) and the height differences between the horizontal faces of the lamellae, corresponding to the lamellar thickness, were measured from the cross sections (see Figure 12a). If the distance between consecutive "steps" formed by lamellae is large enough, such measurements are much more reliable than information based on the profiles of the edge-on lamellae, often employed. The lamellar thickness was also estimated from the height histograms constructed for such terrace structures (Figure 12b). The histograms, representing the share of all points of a given height in the total area chosen, can be regarded as the averaged measurements on the cross sections along all directions in the specimen plane. The distance between the neighboring peaks corresponds to the average thickness of the platelets. The values of the lamellar thickness obtained for both above methods are consistent and equal 20 nm for PECE and PEref melt-crystallized samples.

Therefore, the thickness of the lamellae is the same in samples crystallized from melt with lowered entanglement concentration and from normally entangled melt.

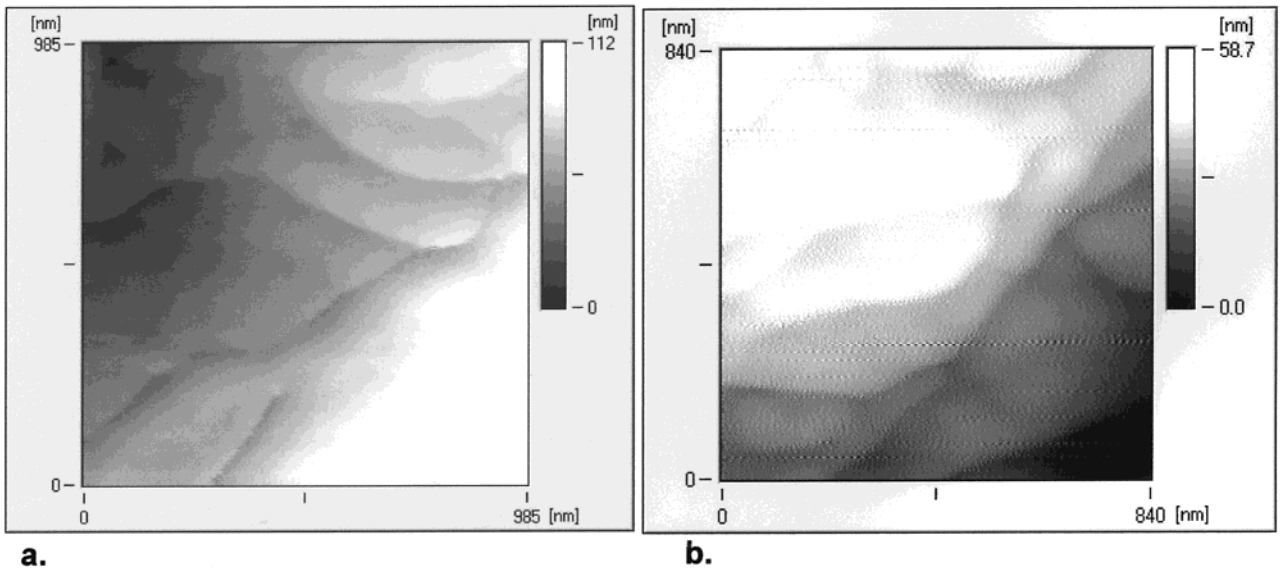

Figure 11. Lamellar structure in PEref (a) and PECE (b) samples crystallized isothermally at 123 °C as revealed by AFM observation.

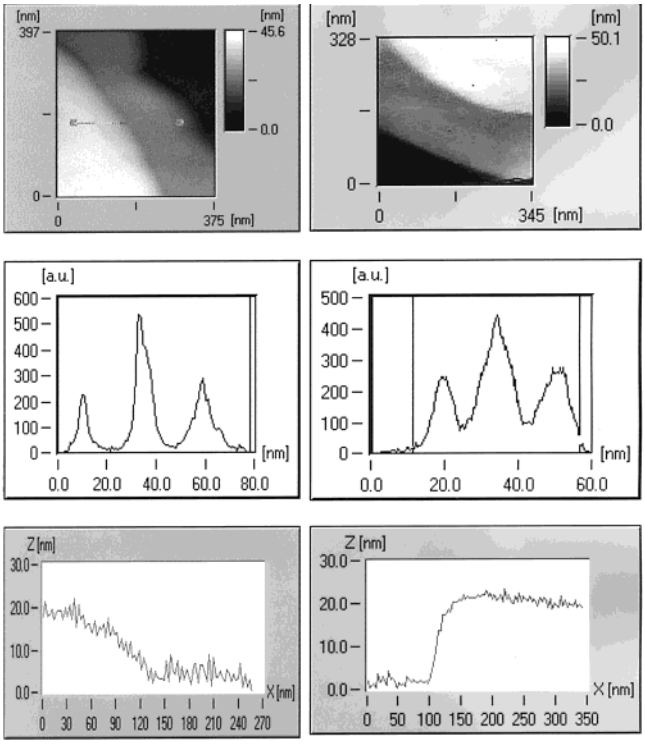

Figure 12. AFM lamellae thickness measurements for PECE (a) and PEref (b) samples: lamellae flat-on, histogram, and height profile.

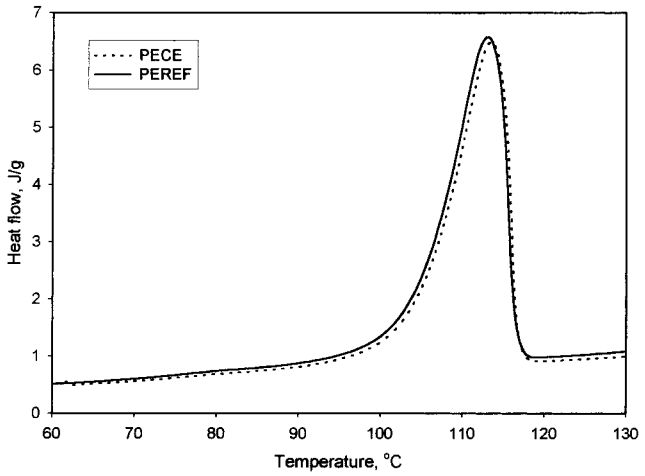

Figure 13. DSC thermograms of polyethylene PECE and PEref samples cooled from 160 °C with a rate of −20 °C/min.

A conclusion that can be drawn from these results, obtained by three independent techniques, is that the extent of entanglement in crystallizing melt is irrelevant to the thickness of the polymer crystals that are formed, although it influences the growth rate and the degree of crystallinity. It is then shown that the thickness of polymer crystals is not controlled by such kinetic factors as entanglements.

Nonisothermal Crystallization. For isothermal crystallization at 123 °C (regime II of crystrallization) PECE samples crystallize faster than PEref samples due to faster spherulite growth rate but in spite of the lower concentration of primary nuclei.

Nonisothermal crystallization proved to occur within a similar temperature range for disentangled and entangled melts on cooling at −20 °C/min. (Figure 13). Also the maxima of the crystallization curves, corresponding to the highest conversion rate, are located at nearly the same temperatures for that cooling rate. PEref samples show similar crystallinity as PECE samples, as it is determined from heat of fusion (68.4% for PEref and 68.9% for PECE samples). With that cooling rate most of the crystallization takes place in the upper part of regime III, where the macromolecules are only slightly pulled from the melt by crystallization forces and the spherulite growth rate in PECE samples is only slightly increased due to disentanglement.

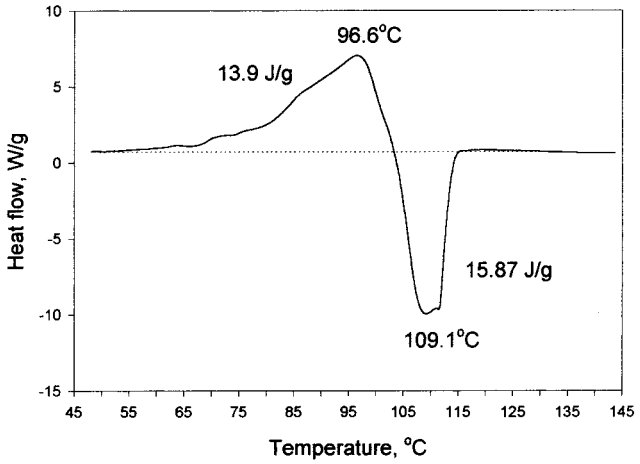

Figure 14. True differential thermograms of polyethylene PECE and PEref samples cooled from 160 °C with a rate of −70 °C/min. Exo is for PECE while the endo direction is for crystallization of PEref samples.

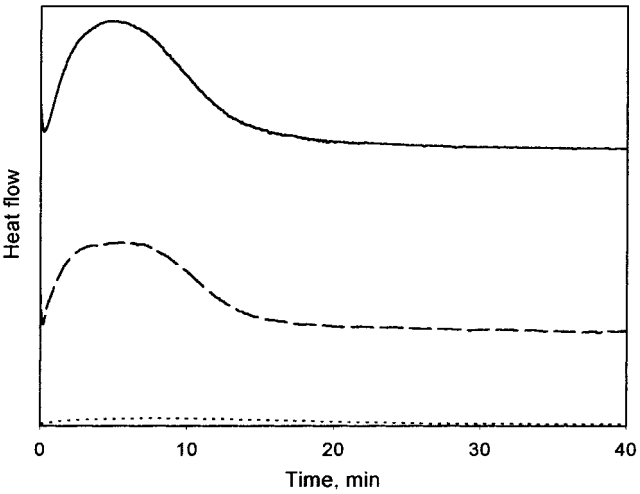

Figure 15. DSC thermograms recorded during isothermal crystallization of HDPE Petrothene at 123 °C, illustrating the influence of high-pressure crystallization conditions (pressure, temperature, and time) on thermal degradation of the polymer, exhibiting lowered crystallization ability. The curves correspond to the following pressure cell conditions: (—) 235 °C, 630 MPa, 1 h; (- - -) 257 °C, 630 MPa, 4 h; (···) 257 °C, 0 MPa, 4 h.

With higher concentration of primary nuclei the PEref samples crystallize with a rate similar to the rate for PECE samples.

Nonisothermal crystallization with a faster cooling rate of −70 °C/min starts earlier and is completed faster in PEref samples than in PECE samples (see Figure 14 where the true differencial thermogram is depicted). Most of the crystallization is finished before massive homogeneous nucleation onset at a temperature of 86−88 °C.[36,37] In spite of different temperature ranges of crystallization, the crystallinity degrees are very similar

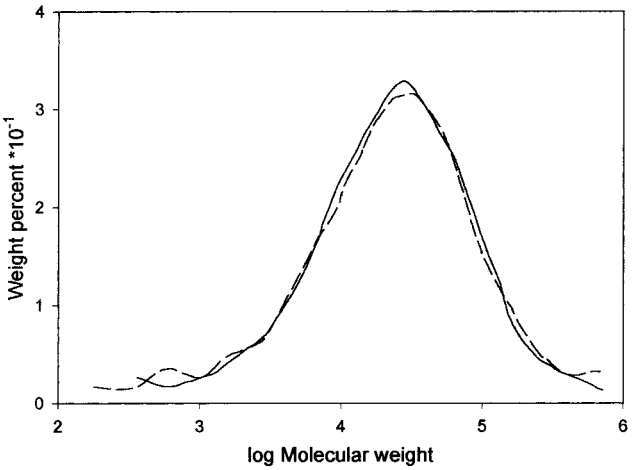

Figure 16. GPC traces recorded for HDPE Petrothene after high-pressure crystallization: (—) 235 °C, 630 MPa, 1 h (PECE sample); (- - -) 235 °C, 250 MPa, 1 h (PEref sample).

for both types of samples (heat of fusion for both samples at the level of 204 J/g and the peak melting temperature of 132.9 °C).

Conclusions

The possibility of obtaining a linear polyethylene melt in which the macromolecular chains are disentangled is shown on the basis of the reptation theory and is verified experimentally. The chains in polyethylene before melting are disentangled owing to chain extension, occurring in pseudohexagonal *condis* mesophase during previous high-pressure crystallization of the samples. Large chain-extended crystals contain no entanglements, and the degree of crystallinity of such material is very high (about 93 wt %). Because the CE crystal basal surfaces contain very few chain folds, it is suggested that on melting the chains are subject to the entropy driven coiling only, which does not increase markedly the number of tight entanglements.

The optimal conditions of the high-pressure crystallization are determined, taking into account the maximal resulting chain extension and the minimal degradation that may affect the samples.

The crystal growth rate in regime II melt crystallization is shown—on the basis of the crystallization theory including reptation—to be sensitive to the extent of melt entanglement. The growth rate measured during isothermal crystallization from melts of chain-extended samples proved to be significantly higher than in the case of reference entangled samples.

The time for a complete re-entangling of the melt is evaluated as 20−30 min, on the basis of spherulite growth rate dependence on the time of previously disentangled melt annealing at 160 °C. Restoring of the spherulite growth rate to its normal level in chain-disentangled samples requires approximately 45 min at 126 °C. It follows that renewing of chain entanglement at 126 °C occurs over a longer time than at 160 °C in the melt-annealing experiment. The activation energy for reptation, determined from these data, is roughly 25 kJ/mol.

Preparation of disentangled samples—via high-pressure crystallization—is supposed to inactivate a large part of the heterogeneous nuclei: a decrease in primary nucleation density in crystallization from the disentangled melt with respect to normally entangled samples is observed. Melt annealing of chain-disentangled samples led to reestablishment of the number of primary nuclei to the level characteristic for reference entangled polyethylene. At 160 °C the nuclei concentration recovers after 25−30 min of melt annealing. The possible reason for lower concentration of nuclei in chain-disentangled polyethylene is the high mobility of macromolecules in the *condis* phase under high pressure. Since primary nuclei in polyethylene active above 90 °C have heterogeneous character, then due to increased chain mobility macromolecules desorb from impurities and most of the heterogeneous nuclei lose their activity. Melt annealing at atmospheric pressure renews the adsorption of macromolecules on impurities, and the nuclei concentration is restored to its regular level. The 25−30 min required for nuclei recovery at 160 °C is the time necessary for significant displacement of macromolecules in the melt by thermal reptation (tube renewal).

The differences between overall isothermal crystallization of PECE and PEref samples are considerable at moderate undercooling. In spite of significantly lower number of primary nuclei, the samples with disentangled chains crystallize faster than the reference chain-entangled samples. The difference results from faster crystal growth rate in chain-disentangled polyethylene.

At larger undercooling, in nonisothermal crystallization with the cooling rate from −20 to −70 °C/min, the differences between chain-disentangled and chain-entangled polyethylene samples are low. It results from the following facts:

(i) The vast portion of crystallization occurs in regime III of crystallization in which the chain fragments moved by crystallization forces are shorter than the chain fragments between the entanglement knots.

(ii) The differences in heterogeneous nucleation become less evident at a faster cooling rate.

The morphology of samples crystallized from the chain-disentangled melt is significantly different than those crystallized from the chain-entangled melt. Nonbanded structures are seen in PECE samples while well-developed banded spherulites are characteristic for samples with saturated entanglement density. At the higher resolution obtained by AFM, it is seen that the internal structure of PECE spherulites is coarser and spherulite centers are visible, but radial arrangement is less than perfect and the interspherulitic borders are not well discernible in all directions with respect to the spherulite centers.

Long periods determined for both types of samples are equal: approximately 34 nm independently of the method of determination, SAXS or AFM. The crystal size determined from AFM is also consistent with these data if the crystallinity degree is taken into account. It seems then that the thicknesses of lamellae as formed during crystallization are not controlled by such kinetic factors as entanglements.

Acknowledgment. This work was supported in part by the State Committee for Scientific Research of Poland, Ph.D. Grant T08E/95/08. The authors are grateful to Professor J. Vancso and Dr. D. Trifonova from University of Twente, Enschede, The Netherlands, for the possibility of performing atomic force microscopy and their assistance in atomic force microscopy of PE samples with chain-extended crystals.

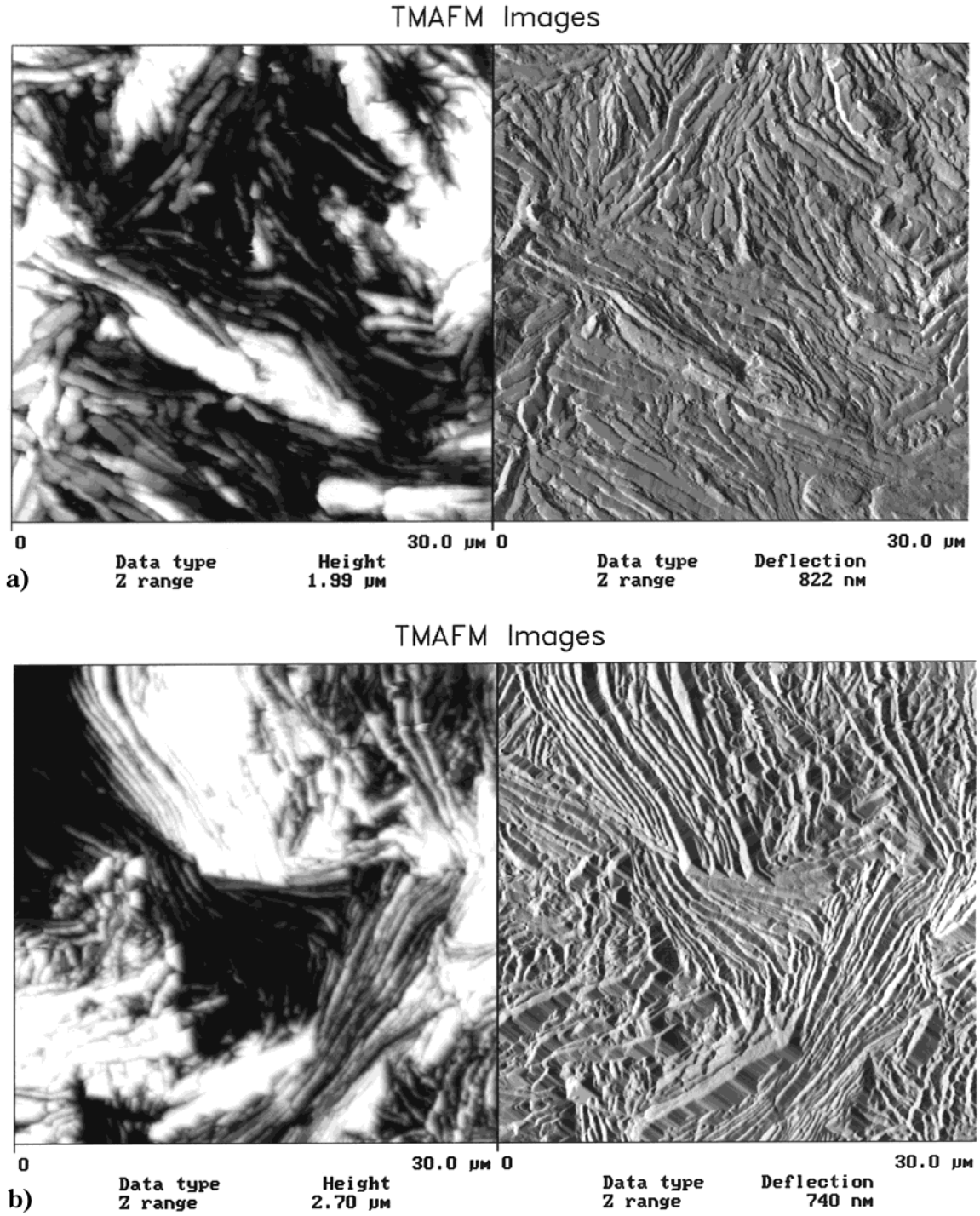

Figure 17. Height and deflection AFM images of etched surfaces of (a) PECE from HDPE Petrothene and (b) PECE from the 88 500 fraction

Appendix I. Experimental Precautions

Two important side effects were considered when measuring spherulite growth rate.

1. Regions of negative pressure in the melt have been previously observed during crystallization of thin polypropylene and polyethylene films, placed between two microscope glasses.[31] Negative hydrostatic pressure, caused by melt deficiency in regions closed by impinged growing spherulites, leads to local growth rate lowering.[38] The possibility of negative-pressure-induced growth rate lowering was taken into account, and the measurements were limited to the specimen regions of evidently unrestricted melt inflow, i.e., a single spherulite or a group of spherulites with no pockets of melt surrouded by growing spherulites.

2. The crystallization process can be also affected if crystallizing melt is subjected to shear.[39] There are two possible sources of shear in the measurements' conditions. If the region of melt deficiency is located near the specimen border, an influx is likely to occur, causing a local melt flow and shear. A fast temperature change may also cause significant shear in polyethylene melt in contact with microscope glass—because of a difference in thermal expansion coefficients of the two. The rate at which the specimens were cooled to the crystallization temperature (−15 °C/min) was therefore a compromise

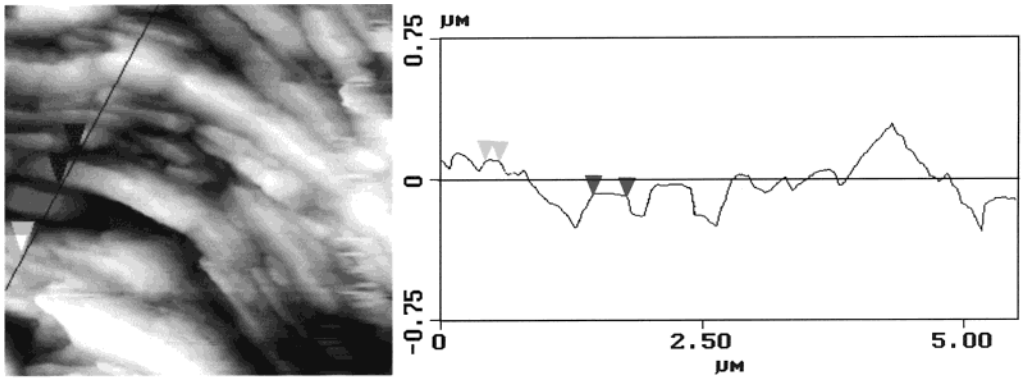

Figure 18. Exemplary lamellar thickness measurement for the high-pressure crystallized HDPE Petrothene sample, performed on the basis of the height line profile.

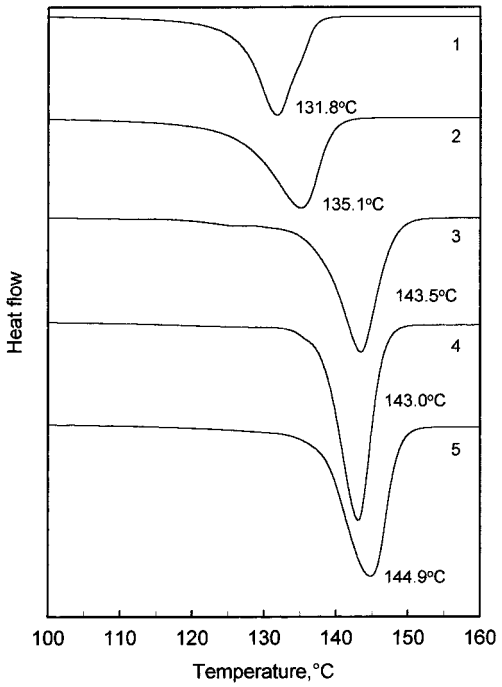

Figure 19. DSC endotherms recorded during heating the polyethylene samples at 10 °C/min: (1) virgin HDPE Petrothene, (2) PEref HDPE Petrothene, (3) PECE HDPE Petrothene, (4) PECE obtained from the 38 400 HDPE fraction, and (5) PECE obtained from the 88 500 HDPE fraction.

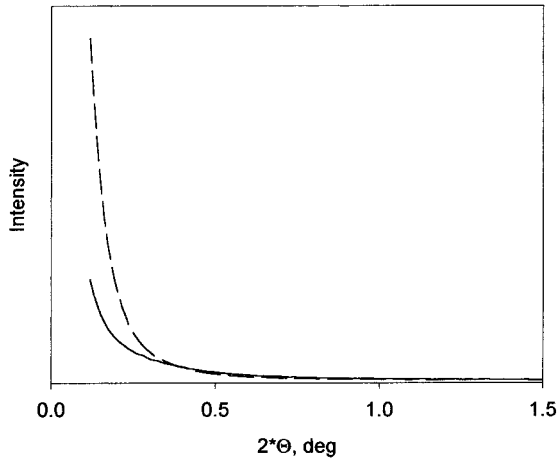

Figure 20. SAXS profiles recorded for PECE from Petrothene (—) and PECE from the 88 500 fraction (- - -).

Table 2. Values of Number and Weight Molecular Weight Averages, M_n and M_w, Respectively, and Polydispersity Indexes, As Determined from GPC Analysis of HDPE Petrothene Samples, Virgin, PECE, and PEref

sample	$M_n \times 10^{-3}$	$M_w \times 10^{-3}$	M_w/M_n
virgin polymer	11.7	55.5	4.77
PECE	13.2	58.1	4.40
PEref	12.2	56.4	4.64

between the desired reduction of time needed to reach the T_c after melt annealing (2.6 min in the case of cooling from $T_{ann} = 160$ °C to $T_c = 121$ °C, at a rate of −15 °C/min) and the necessity of eliminating the effect of shear in cooled melt.

Because of the above effects, specimens suitable for accurate growth rate measurements were carefully chosen and a suitable number of measurements were performed, so as to ensure the satisfactory statistics of the results.

3. A prolonged exposure of polymer to high temperature may cause various degradation reactions like depolymerization, cross-linking, or thermal oxidation, leading to polymer molecular weight modification or microgel formation. In the case of polyethylene, the molecular weight lowering caused by depolymerization becomes significant at temperatures above 290 °C, which exceeds the temperature range applied in this study. The thermal oxidation on the other hand, although it takes place at much lower temperatures (heating polyethylene at 190 °C for 2 h causes significant molecular weight modifications), is stopped by antioxidants present in the commercial grade polyethylene used in this research. The oxidation tests, conducted according to the European Norm EN 728, showed that this polymer is thermally stable in an oxygen atmosphere at 190 °C for about 10 min. During high-pressure crystallization, very tight sealing of the cell eliminates the access of the oxygen to the sample. It is thus expected that the antioxidants present in the sample efficiently stop the oxidation caused by slight amounts of oxygen remaining in the sample after compression. The oxidation tests conducted after crystallization at the conditions given above (235 °C, 630 MPa, 1 h) show that a substantial amount of antioxidants still exist in a sample. This implies that thermal oxidation did not occur during high-pressure crystallization. A higher crystallization temperature or longer crystallization time result in a loss of thermal oxidation resistance, which indicates that some degradation might have happened in these cases. The extent of degradation was also monitored by means of isothermal crystallization runs performed in the DSC apparatus. The crystallization ability of a sample, reflected by the magnitude

Table 3. Values of the Lamellar Thickness, *l, Estimated on the Basis of the DSC Melting Peak Position, T_m, Compared to the Relevant Fully Extended Chain Lengths, l_{max}[a]**

sample	M_w	T_m^0, °C	T_m, °C	l^*, nm	l_{max}, nm	X_c, wt %
			PE-HD Petrothene			
virgin polymer	55 000	145.1	131.8	20	100	61.5
PEref	55 000	145.1	135.1	30	100	72.5
PECE	55 000	145.1	143.5	170	100	92.3
			PE-HD Fractions			
	38 400	144.3	143.0	210	320	90.0
	88 500	145.3	144.9	670	740	91.0

[a] The values of the equilibrium melting temperature are estimated from the Hoffman−Weeks plot for the HDPE Petrothene and interpolated from the data by Hoffman et al.,[41] of T_m^0 for fractions, assuming $T_m^0(\infty) = 146.0$ °C. The degree crystallinity, X_c, is evaluated on the basis of the DSC thermograms.

Table 4. Crystallographic Data Obtained from Deconvolution Analysis of WAXS Patterns for PE-HD Petrothene Samples

sample	crystallographic plane	peak position 2θ, deg	peak width, deg	crystallinity, %
virgin polymer	(110)	21.6	0.13	
	(200)	24.1	0.18	74
	(010)[a]	19.4	0.11	
	(110)	21.6	0.09	
	(200)	24.1	0.11	86
	(010)[a]	19.3	0.07	
PECE 88 500	(110)	21.6	0.07	
	(200)	24.2	0.10	87
	(010)[a]	19.4	0.07	

[a] Triclinic form.

of the exothermal effect recorded during crystallization, proved to decrease with increasing severity of the previous thermal treatment (Figure 15).

The set of high-pressure crystallization parameters chosen for the preparation of samples used in further study ensured the minimum extent of degradation that might have affected the CE material.

The GPC measurements were performed using a Waters 150-C apparatus equipped with a differential refractometric detector and Waters HMW-7 and HMW-6E columns at 142 °C. Samples were dissolved in 1,2,4-trichlorobenzene at 142 °C for 25 h. The analysis, performed on PECE and PEref samples—see Figure 16 and Table 2—confirmed that high-pressure conditions chosen in this work do not cause any significant changes in the molecular weight distribution (within experimental error). The slight increase in M_n is attributable to filtration of microgels during the GPC experiments.

Appendix II, Characterization of PECE and PEref Samples

The morphological features of high-pressure crystallized material, as revealed by atomic force microscopy (see Figure 17), are characteristic of CE polyethylene crystals, investigated earlier in detail by Bassett and co-workers[27] and—more recently—by Wunderlich and co-workers.[28] Randomly oriented stacks of thick lamellae and a lack of any radial (spherulitic) arrangement of crystals are typical for these samples. The average lamellar thickness, *l**, estimated on the basis of the topographical line profiles (Figure 18), is on the order of 380 nm for the Petrothene PECE samples.

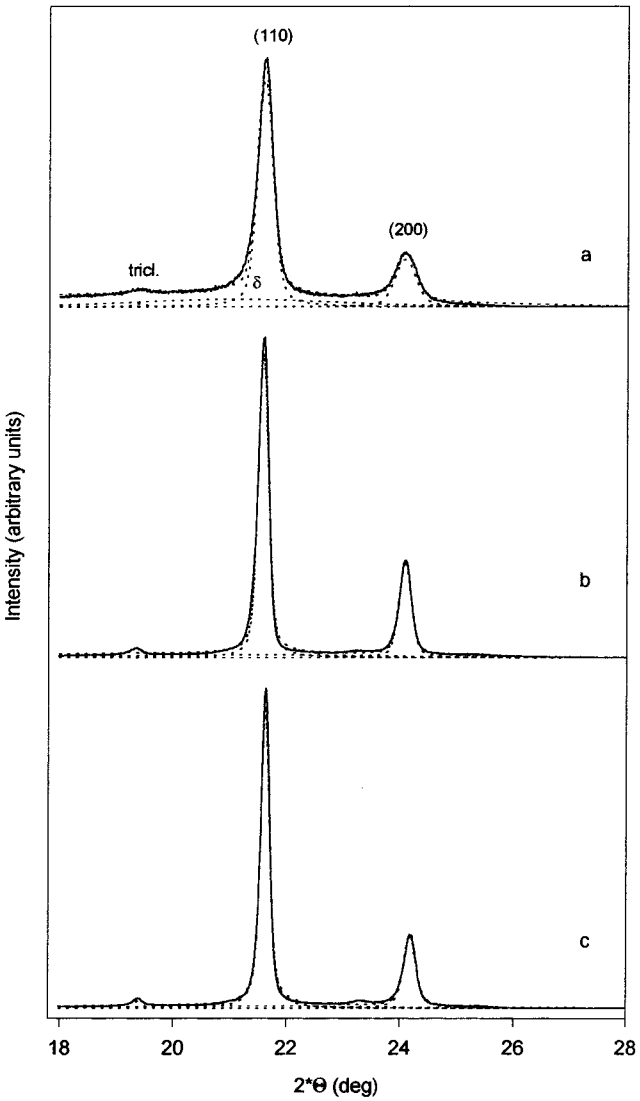

Figure 21. WAXS profiles and separated peaks: (a) virgin HDPE Petrothene film; (b) PECE obtained from HDPE Petrothene crystallized at 235 °C, 630 MPa; (c) PECE obtained from the HDPE 88 500 fraction crystallized at 237 °C, 630 MPa. Key: (—) experimental profile; (···) calculated profile and resolved peaks. Peaks correspond to the orthorhombic and triclinic phases of PE. The crystallographic planes are indexed in parentheses; the amorphous halo of each sample is labeled with δ.

The average lamellar thicknesses of the PECE and PEref samples were also determined, in a more comprehensive way, by means of the DSC melting records. In Figure 19, a set of endotherms recorded for various types of samples is shown. The values of *l**, calculated on the basis of eq 3, are presented in Table 3. The crystal thicknesses are compared to the relevant fully extended chain lengths for polyethylene of $M_w = 55\,000$, which was used in this work.

The remarkable increase in the melting temperature at atmospheric pressure of the pseudohexagonal phase grown crystals is due to their high thickness—the depression of T_m, resulting from their nonequilibrium size, is much lower than in the case of polyethylene crystallized under normal conditions. The comparison of the lamellar thicknesses with pertinent chain lengths indicates that a major part of high-pressure formed crystals contains completely or largely extended macromolecular chains. Also their degrees of crystallinity,

shown in Table 3, are very high (over 92 wt %).

The additional characterization of the PECE and PEref samples involved basic SAXS and WAXS structural analysis and a density-based crystallinity level determination.

No maxima can be resolved in the SAXS diffractograms recorded for the PECE samples (see Figure 20). As the lamellar morphology of the samples was demonstrated by the AFM images, it is reasonable to consider that the long period that could be detected by the SAXS measurements exceeds the experimental setup resolution (80 nm).

The WAXS profiles recorded were subject to a procedure of separation of the amorphous halo and reflections originating from main crystallographic planes of the lattice. The deconvolution program, described in detail in refs 24 and 40, allows one to calculate—within a predetermined range—the positions of the reflections, their widths and heights, and, consequently, the degree of sample crystallinity. The experimental profiles and separated peaks are shown in Figure 21. The profiles are typical for a polyethylene orthorhombic unit cell. The positions and half-widths of three resolvable reflections, corresponding to the diffraction on the (110) and (200) planes of the orthorhombic system and the (010) plane of the triclinic system are listed in Table 4. Also, the degrees of crystallinity of the samples, calculated as the ratio of the sum of integrated intensities of the reflections coming from the crystalline phase to the total scattered intensity (corrected for absorption, polarization, and background) are shown in this table. The crystalline reflections of the high-pressure crystallized samples are much narrower than those of virgin polymer and only slightly overlap. Thus, the perfection of crystals in PECE samples is much higher than in regular polyethylene; the same also holds for the degree of crystallinity.

The degrees of crystallinity of the PECE and PEref samples, calculated on the basis of the density measurements (assuming the densities of the crystalline phase, $\rho_c = 1.0020$ g/cm^3, and of the amorphous phase, $\rho_a = 0.8531$ g/cm^3 (ref 41), evidenced that the PECE samples are highly crystalline: $X_c^{PECE} = 93.0$ wt % and $X_c^{PEref} = 75.6$ wt %, respectively.

References and Notes

(1) Barham, P. J.; Sadler, D. M. *Polymer* **1991**, *32*, 393.
(2) Raju V. R.; Smith, G. G.; Martin, G.; Knox, J. R.; Graessley, W. W. *J. Polym. Sci., Polym. Phys. Ed.* **1979**, *17*, 1183
(3) Cassagnau, P.; Montfort, J. P.; Martin, G.; Monge, P. *Rheol. Acta* **1993**, *32*, 156.
(4) de Gennes, P. G.; *Scaling Concepts in Polymer Physics*; Cornell University Press: Ithaca, NY, and London, 1979.
(5) de Gennes, P. G. *J. Chem. Phys.* **1971**, *55*, 572.
(6) Edwards, S. F. *Proc. Phys. Soc.* **1967**, *92*, 9.
(7) Doi, M., Edwards, S. F. *J. Chem. Soc., Faraday Trans. 2* **1978**, *74*, 1789, 1802, 1818.
(8) Graessley, W. W. In *Macromolecular Conformation and Dynamics of Macromolecules in Condensed Systems*; Nagasawa, N., Ed.; Studies in Polymer Science Series; Elsevier: Amsterdam, Oxford, England, New York, and Tokyo, 1988, Vol. 2, p 163.
(9) Graessley, W. W. *Adv. Polym. Sci.* **1982**, *47*, 67.
(10) Doi, M. In *Structure and Properties of Polymers*; Cahn, R. W., Haasen, P., Kramer, E. J., Eds.; Materials Science and Technology Series, VCH: Weinheim, Germany, New York, Basel, Switzerland, Cambridge, England, and Tokyo, 1993; Vol. 12, Chapter 9.
(11) Gell, C. B.; Graessley, W. W.; Fetters, L. J. *J. Polym. Sci., Part B: Polym. Phys.* **1997**, *35*, 1933
(12) Bastiaansen, C. W. M. Ph.D. Thesis, Eindhoven University of Technology, 1991.
(13) Rastogi, S.; Spoelstra, A. B.; Goosens, J. G. P.; Lemstra, P. J. *Macromolecules*, **1997**, *30*, 7880
(14) Turnbull, D.; Fisher, J. C. *J. Chem. Phys.* **1949**, *17*, 71.
(15) Hoffman, J. D.; Davis, G. T.; Lauritzen, J. I., Jr. In *Treatise on Solid State Chemistry*,; Hannay, N. B., Ed.; Plenum Press: New York, 1976; Vol. 3, Chapter 7.
(16) Hoffman, J. D. *Polymer* **1982**, *23*, 656.
(17) Hoffman, J. D. *Polymer* **1983**, *24*, 3.
(18) Hoffman, J. D.; Miller, R. L. *Polymer* **1997**, *38*, 3151.
(19) Hikosaka, M. *Polymer* **1987**, *28*, 1257; **1990**, *31*, 458.
(20) Kowalewski, T.; Galeski, A. *J. Appl. Polym. Sci.* **1992**, *44*, 92.
(21) Lauritzen, J. I.; Hoffman, J. D. *J. Res. Natl. Bur. Stand.* **1960**, *64A*, 73.
(22) Hoffman, J. D., Lauritzen, J. I. *J. Res. Natl. Bur. Stand.* **1961**, *65A*, 297.
(23) Stamm, M.; Fisher, E.; Dettenmaier, M. *Faraday Discuss. Chem. Soc.* **1979**, *68*, 263
(24) Psarski, M.; Pracella, M.; Galeski, A. *Polymer* **1999**, in press.
(25) Sheiko, S. S.; Moller, M.; Keuvekamp, E. M. C. M.; Zandbergen, H. W. *Phys. Rev., Part B* **1993**, *48*, 5675
(26) Maxfield, J.; Mandelkern, L. *Macromolecules* **1977**, *10*, 1141.
(27) Bassett, D. C. In *Developments in Crystalline Polymers*; Bassett, D. C., Ed.; Applied Science Publishers: London, 1982; Vol. 1, Chapter 3.
(28) Annis, B. K.; Reffner, J. R, Wunderlich, B. *J. Polym. Sci.: Part B: Polym. Phys.* **1993,** *31*, 93
(29) Hoffman, J. D.; Frolen, L. J.; Ross, G. S.; Lauritzen, J. I., Jr. *J. Res. Nat. Bur. Stand. (U.S.)* **1975**, *79A*, 671
(30) Klein, J.; Briscoe, B. J. *Proc. R. Soc. London, A* **1979**, *365*, 53.
(31) Piorkowska, E.; Galeski, A. *J. Polym. Sci., Part B.: Polym. Phys.* **1993,** *31*, 1285
(32) Wu, S. *Polymer Interface and Adhesion*; Marcel Dekker: New York and Basel, Switzerland, 1982; p 205.
(33) Malinowski, P.; Galeski, A. *Preprints of 3rd Euro-American Conference on Functional Polymers and Biopolymers*; University of Kent: Canterbury, U.K., 1992. See also: Galeski, A.; Psarski, M. *Macromol. Symp.* **1996**, *104*, 183.
(34) Billon, N.; Magnet, C.; Haudin, J. M.; Lefebvre, D. *Colloid Polym. Sci.* **1994,** *272*, 633.
(35) Piorkowska, E. *Colloid Polym. Sci.* **1997**, *275*, 1035; **1997**, *275*, 1046.
(36) Koutsky J. A.; Walton A. G.; Baer, E. *J. Appl. Phys.* **1967**, *38*, 1832.
(37) Cormia R. L.; Price F. P.; Turnbull, D. *J. Chem. Phys.* **1962**, *37* 1333.
(38) Pawlak, A, Galeski, A, *J. Polym. Sci., Part B.: Polym. Phys.* **1990**, *28*, 1813.
(39) Thomason, J. L., van Rooyen, A. A. *J. Mater. Sci.* **1992**, *27*, 889, 897.
(40) Galeski, A.; Bartczak, Z.; Argon, A. S.; Cohen, R. E. *Macromolecules* **1992**, *25*, 5707.
(41) Jackson, J. B.; Flory, P. J.; Chiang, R. *Trans. Faraday. Soc.* **1963**, *59*, 1906.

MA990298H